



RESEARCH ARTICLE

10.1029/2019SW002281

Key Points:

- All rates of change ≥ 200 nT/min occur within 3 days of a sudden commencement
- Less than 8% of potentially damaging rates of change occur during sudden commencements
- Over 90% of all extreme rates of change occur within 3 days of a sudden commencement

Correspondence to:

A. W. Smith,
andy.w.smith@ucl.ac.uk

Citation:

Smith, A. W., Freeman, M. P., Rae, I. J., & Forsyth, C. (2019). The influence of sudden commencements on the rate of change of the surface horizontal magnetic field in the United Kingdom. *Space Weather*, 17, 1605–1617. <https://doi.org/10.1029/2019SW002281>

Received 14 JUN 2019

Accepted 25 OCT 2019

Accepted article online 9 NOV 2019

Published online 21 NOV 2019

This article was corrected on 1 JUN 2020. See the end of the full text for details.

©2019. The Authors.

This is an open access article under the terms of the Creative Commons Attribution License, which permits use, distribution and reproduction in any medium, provided the original work is properly cited.

The Influence of Sudden Commencements on the Rate of Change of the Surface Horizontal Magnetic Field in the United Kingdom

A. W. Smith¹ , M. P. Freeman² , I. J. Rae¹ , and C. Forsyth¹

¹Mullard Space Science Laboratory, UCL, Dorking, UK, ²British Antarctic Survey, Cambridge, UK

Abstract Sudden commencements (SCs) are rapid increases in the northward component of the surface geomagnetic field, related to sharp increases in the dynamic pressure of the solar wind. Large rates of change of the geomagnetic field can induce damaging currents in ground power networks. In this work, the effect of SCs on the (1 min) rate of change of the surface magnetic field (R) at three U.K. stations is investigated. The distributions of R during SCs are shifted to higher values than the data set as a whole. Rates of change greater than 10 nT/min are 30–100 times more likely during SCs, though less than 8% of the most extreme R (≥ 99.99 th percentile) are observed during SCs. SCs may also precede geomagnetic storms, another potential source of large R . We find that the probability of observing large a R is greatly enhanced for 3 days following an SC. In the 24 hr following an SC it is 10 times more likely than at any given time to observe rates of change between 10 and several hundred nT/min. Additionally, between 90% and 94% of data (depending on station) above the 99.97th percentile is recorded within 3 days of an SC. All values of $R \geq 200$ nT/min in the United Kingdom have been observed within 3 days of an SC. These results suggest that accurately predicting SCs is critically important to identify intervals during which power networks at similar geomagnetic latitudes to the United Kingdom are at risk from large geomagnetically induced currents.

1. Introduction

As a consequence of Faraday's law, temporal variations in a magnetic field will result in an induced electric field. Thus, temporal variations in Earth's surface magnetic field, caused by currents flowing through the upper atmosphere and in the magnetosphere, create electric potential differences across the Earth's surface. Consequently, currents will flow through conductors connected to the ground, such as power lines (Lehtinen & Pirjola, 1985). Such externally sourced currents in power networks, known as geomagnetically induced currents (GICs), can distort the waveforms inside transformers, potentially leading to damage (Boteler, 2003; Boteler et al., 1998; Kappenman, 2005). Indeed, sufficiently large rates of change of the geomagnetic field, and the resulting large GICs, can disrupt power networks. The most famous example of this is the Hydro-Quebec blackout in March 1989 (Bolduc, 2002).

The exact magnitude of GICs at any given location depends on the precise configuration of the power network, variations in the local ground conductivity, and the rate of change of the surface magnetic field (Beggan, 2015; Boteler, 2014; Thomson et al., 2005; Viljanen et al., 1999, 2013, 2014) with larger rates of change of the surface magnetic field driving larger GICs in a given network (Bolduc et al., 1998; Viljanen et al., 2001). For example, during the Hydro-Quebec event in 1989 the maximum ground magnetic field change measured was 479 nT/min, though significant GICs have been observed for values as low as 100 nT/min at other locations (Kappenman, 2003, 2006).

The largest ground magnetic field perturbations are most often associated with geomagnetic storms (Kappenman, 1996; Kappenman & Albertson, 1990); indeed, storms may be defined by magnetic indices that are derived from the observed range of surface field observations (e.g., A_p or K_p). Storms themselves often commence with a rapid increase in solar wind dynamic pressure (Araki, 1977, 1994; Chapman & Ferraro, 1931, 1932). Physically, these rapid pressure changes correspond to a shock, usually found at the interface between the fast and slow solar wind streams (a corotating interaction region, CIR), or ahead of a coronal mass ejection (CME), a massive eruption of solar material. In addition

to potentially causing a geomagnetic storm, a large increase in solar wind dynamic pressure will also enhance magnetopause currents, causing a sudden increase in the strength of the horizontal (H) component of the geomagnetic field at the ground. When observed in ground magnetometer data, this increase in H is known as a sudden commencement (SC) (Chree, 1925; Fiori et al., 2014; Lühr et al., 2009; Takeuchi et al., 2002). SCs can be further subdivided into two categories: storm sudden commencements (SSCs) and sudden impulses (SIs), which share the same physical origin (Curto et al., 2007). If the sharp increase in the H component is followed within a few hours by a geomagnetic storm, then it is termed an SSC, and if a storm is not initiated, then it is known as an SI.

Observations of the solar wind and interplanetary space may enable the prediction of the impact of CIRs and CMEs and consequently the prediction of SCs. CIRs are linked to the fast solar wind originating from coronal holes and recur with a ~ 27 day period (e.g., Gosling & Pizzo, 1999; Bothmer et al., 1999). On shorter timescales (~ 1 day), the progress of CMEs through interplanetary space can be tracked (e.g., Harrison et al., 2017) and modeled (e.g., Zhao & Dryer, 2014). Finally, with an even shorter lead time (< 1 hr), the structures may be observed by ACE or WIND at L1 prior to impact. These methods enable forecasting and are therefore useful from the perspective of predicting adverse space weather effects, that is, potential GICs from SCs and the following geomagnetic storms.

As mentioned above, large rates of change of the geomagnetic field are most often associated with the intensification of auroral currents during geomagnetic storms and substorms (e.g., Kappenman & Albertson, 1990; Kappenman, 1996; Pulkkinen et al., 2005; Pulkkinen et al., 2012; Ngwira et al., 2013; Freeman et al., 2019). However, the United Kingdom covers a range of latitudes between $\sim 45^\circ$ and 60° and therefore does not often observe the direct effects of the auroral current systems. SCs meanwhile are a global phenomena, and their adverse impact on middle-to-low latitude power grids has been documented (Beland & Small, 2004; Carter et al., 2015; Kappenman, 2003; Marshall et al., 2012; Zhang et al., 2015).

The initial ground response to an SC is complicated, with multiple components that vary with both latitude and local time (e.g., Curto et al., 2007, and references therein). At low latitudes the change in the H component resembles a step function, caused by the increase in the magnetopause currents. Near the equator this signature may be complicated by enhancements of the equatorial electrojet (Carter et al., 2015). Meanwhile, at high latitudes the change in H shows a two-pulse structure, theorized to be caused by field-aligned and ionospheric currents (Araki, 1977, 1994). The latitude at which this two-pulse structure appears and then dominates is variable, and such a signature can sometimes be observed at middle-to-low latitudes (Araki et al., 2006; Kikuchi et al., 2001). However, for the majority of events, the amplitude of SCs is observed to increase with increasing latitude (Fiori et al., 2014; Lühr et al., 2009).

Recently, Freeman et al. (2019) studied the effects of substorms, an intermittent cycle of energy storage and release in the magnetosphere (Akasofu, 1964; McPherron et al., 1973), on the rate of change of the surface magnetic field (R) at three U.K.-based magnetometer stations. They found that the occurrence frequency of large values of R decreased with decreasing station latitude. Additionally, over half of large (≥ 99 th percentile) and extreme (≥ 99.97 th percentile) values of R were found within substorm expansion and recovery phases, which constituted only 13.4% of the data set. This therefore showed an enhanced risk of large GICs in the U.K. power network during substorm intervals.

Building on the work of Freeman et al. (2019), we examine the influence of SCs on the rate of change of the horizontal ground magnetic field in the United Kingdom. Section 2 will describe the data used and definitions employed by this study. Section 3 will then explore the SC-related rate of change of the magnetic field, in terms of both the immediate impact of SCs and the delayed response of the geomagnetic system. Section 4 will then discuss the results in the context of magnetic latitude and the risk of large GICs in the United Kingdom.

2. Data and Definitions

We use the methodology outlined in Freeman et al. (2019) to investigate the effect of SCs on the surface magnetic field rate of change observed in the United Kingdom. We use data from the three INTERMAGNET observatories located in the United Kingdom, operated by the British Geological Survey. The Hartland observatory (henceforth HAD) is the lowest-latitude station, located in southwest England at (50.995°N ,

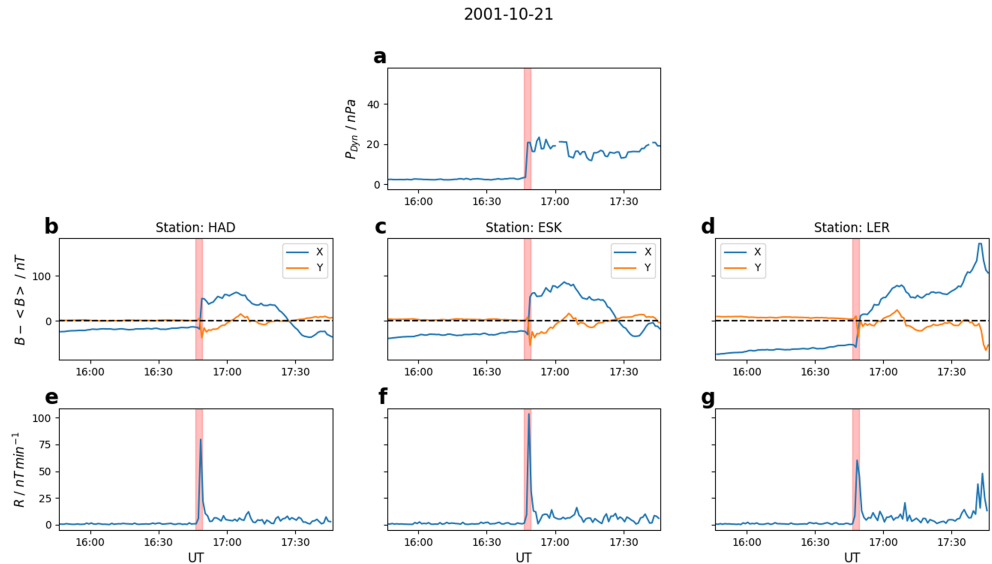


Figure 1. A 2 hr interval showing the impact of a sudden commencement on the horizontal field at three U.K. magnetometer stations. The top panel (a) shows the dynamic pressure of the solar wind from the OMNI database. From left to right, the lower rows show data for each station in turn (HAD, ESK, and LER from left to right). The middle row (b–d) shows the horizontal components of the magnetic field with a 2 hr mean value subtracted, while the bottom row (e–g) shows the rate of change of the horizontal magnetic field, calculated from equation (1). The red bar indicates the duration of the SC from the catalog.

355.516°E) in geographic coordinates. The Eskdalemuir (ESK) observatory is at a higher latitude near England/Scotland border (55.314°N, 356.794°E). Finally, the Lerwick (LER) observatory is the highest latitude station on an island north of mainland Scotland (60.138°N, 358.817°E). The observatories are approximately evenly spaced over the full latitudinal extent of the United Kingdom. We use 1 min averaged data from 1996 to 2016 (inclusive), spanning almost two solar cycles and providing a total of ~ 11 million data per station.

2.1. Rate of Change

In this work we investigate the rate of change of the horizontal component of the surface magnetic field vector $\mathbf{H} = (X, Y)$, where X and Y are the geographic northward and eastward components, respectively. We define the rate of change R as the absolute displacement of \mathbf{H} , as used by Viljanen et al. (2001) and Freeman et al. (2019):

$$R = \frac{\delta \mathbf{H}}{\delta t} = \frac{\sqrt{[X(t + \delta t) - X(t)]^2 + [Y(t + \delta t) - Y(t)]^2}}{\delta t} \quad (1)$$

Other studies have used the rate of change of the magnitude of \mathbf{H} , for example, Thomson et al. (2011). The advantage of our definition is that it captures directional changes of the field when the field magnitude remains constant. Such directional changes can also result in GICs (e.g., Beggan, 2015). With this definition we avoid any assumptions regarding the direction of the currents and their orientation relative to the power network.

2.2. SCs

The International Service on Rapid Magnetic Variations (part of the International Service of Geomagnetic Indices), based at Ebre Observatory, maintains a catalog of SCs dating from 1869 to the present day. The SCs are identified based on the visual inspection of data from a network of five widely spaced, low-latitude magnetic observatories (Curto et al., 2007). The lists for each year can be found online (at: <http://www.obsebre.es/en/rapid>).

For this study we use the event lists covering the same period as the ground-based magnetometer data (1996–2016). Overall this time period contains 380 SCs, comprising a total of $\sim 1,900$ min of data. From 2006 onward the events are already classified as being SSC- or SI-type events. However, this classification is not present for the data between 1996 and 2005, and we therefore apply our own simple criterion to the full cata-

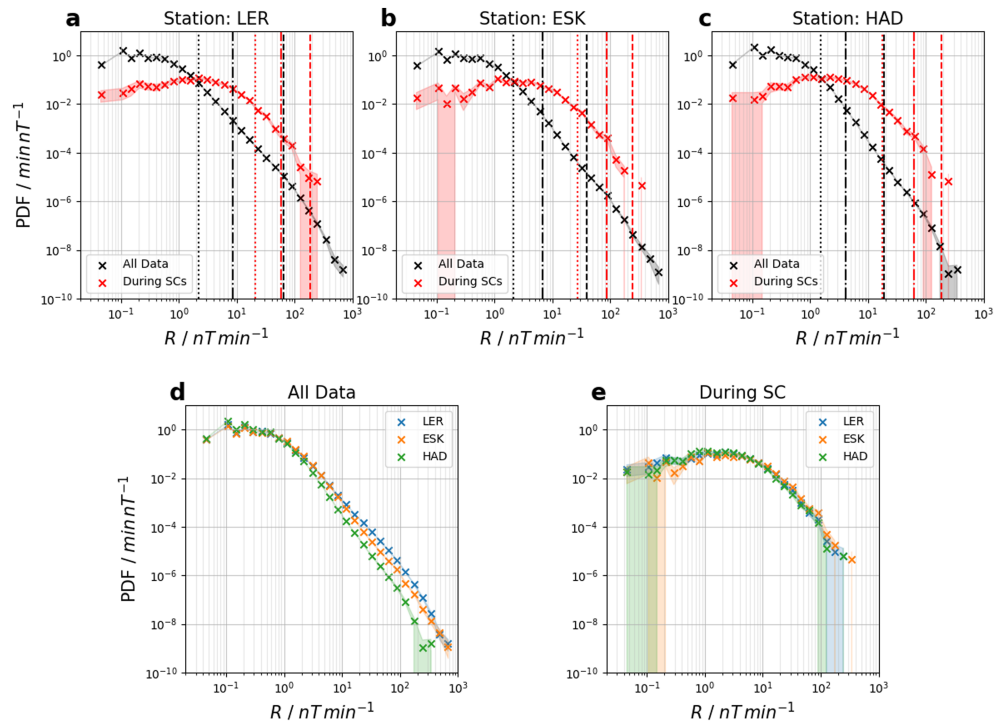


Figure 2. PDFs of R for the HAD (a), ESK (b), and LER (c) magnetic observatories for data obtained between 1996 and 2016 (inclusive). In the top row black and red data represent the PDFs from the total data set and that obtained during SCs, respectively. The vertical dotted, dot-dashed, and dashed lines represent the 90th, 99th, and 99.97th percentiles for each distribution. The shaded region shows the 68.27% confidence interval, assuming the general Poisson distribution. The lower row shows the PDFs for all three stations for the full data set (d) and during SCs (e).

log based upon existing criteria in the literature. If the Sym-H index falls to ≤ 50 T in the 24 hr following the SC then we classify it as an SSC; if it does not then it is classed as an SI. This is similar to other criteria used to define geomagnetic storms (Gonzalez et al., 1994; Reeves et al., 2003; Turner et al., 2015), and SSCs (Curto et al., 2007; Fiori et al., 2014). A large majority of our classifications post-2006 are consistent with their original designation in the catalog: Only 7% are different. These all correspond to events that either showed storm-like activity more than 24 hr after the SC or alternatively showed a K_p enhancement but more modest Dst changes. Our definition of an SSC does not include a criterion regarding changing magnetic “rhythm” (Mayaud, 1973) and therefore may be slightly restrictive; however, it is simple and easily reproducible.

An example SC at the three U.K. stations is shown in Figure 1. The top panel shows the solar wind dynamic pressure as recorded in the OMNI database (<http://nssdc.gsfc.nasa.gov/omniweb/>), containing measurements propagated from the L1 point to the bowshock. The middle row shows the background subtracted horizontal components of the geomagnetic field, while the lower panels show the rate of change: R (using equation (1)). The SC interval identified from the catalog start time and duration is highlighted in red and encompasses a sharp increase in solar wind dynamic pressure, and corresponding rapid changes in the horizontal field at all three U.K. stations, and therefore large values of R . For this particular event the largest value of R is recorded at ESK, while lower values are observed at HAD and LER. We discuss the relative magnitudes of R as a function of latitude below in section 3.1. Note that at HAD the change in the X component is greater than the change in the Y component, indicating a change in both magnitude and direction, justifying our definition of R in section 2.1. In contrast, at LER these changes are more similar in both components, indicating a smaller change in direction.

3. Results

3.1. Statistics of R During SCs

We analyze the statistics of R between the start and end of SCs. Figure 2 shows the probability density functions (PDFs) of R from the (a) HAD, (b) ESK, and (c) LER stations. The binning of the PDF is performed as described by Freeman et al. (2019), with bins algebraically increasing in width and so evenly spaced in

Table 1
Percentiles From Figure 2

	Percentile	HAD	ESK	LER
All	90th	1.5	2.2	2.2
	99th	4.2	6.8	8.4
	99.97th	18.8	38.8	64.2
SC	90th	17.4	26.7	20.5
	99th	61.7	86.5	58.8
	99.97th	182.0	240.6	182.9

Note. Values are provided in units of nT/min.

log R . The black crosses show the PDFs of R from the entire interval under all conditions, while the red crosses show PDFs of the data recorded during the $\sim 19,00$ min of SC activity. The colored vertical lines in Figures 2a–2c show the 90th (dotted), 99th (dot-dashed), and 99.97th (dashed) percentiles of correspondingly colored PDFs. These percentiles were chosen to enable simple comparison with previous results from Freeman et al. (2019). However, given the relatively small size of the SC data set the 99.97th percentile should be treated with some caution. The values of the chosen percentiles are also provided in Table 1.

At all three stations, the probability of the occurrence of $R \leq 1$ nT/min is lower during SCs than for the data set as a whole, and the probability of recording a value of $R \geq 1$ nT/min is higher during SCs. It is worth noting that the PDF at low R (e.g., ≤ 1 nT/min) during SCs will be affected by the detectability of SCs: SC-like events with small rates of change will be less likely to be manually identified and selected. The PDFs cross over each other close to the 90th percentile of all data at each station. At a value of $R \sim 100$ nT/min the PDFs obtained during SCs are approximately 2 orders of magnitude greater than for the overall distribution at HAD and ESK. The difference is approximately 1 order of magnitude at LER.

Examining the full data set, the values of R for the equivalent percentiles increase with latitude meaning that, overall, higher values of R are more likely at LER than at HAD. This is also clearly shown by the PDFs in Figure 2d. This result was previously reported by Freeman et al. (2019), and is likely due to the relative locations of HAD, ESK, and LER to the auroral current systems that reside at high latitudes. In contrast, the percentiles of R during SCs are largest at ESK, while HAD and LER display similar values (to within a few nT/min).

At the lowest latitude station, HAD, the 90th percentile of the SC data set roughly corresponds to the 99.97th percentile of the entire data set. At ESK, the 90th percentile from the SC data set lies between the 99th and 99.97th percentiles from the full data set. Finally, at the highest latitude, LER, the 99th percentile of the SC data set roughly corresponds to the 99.97th percentile of the full data set. These results can be visualized as a large separation between the PDFs at large R in Figure 2a and increasingly small separations moving to Figures 2b and 2c. Therefore, as you move toward lower latitudes a greater fraction of the large and extreme values of R occur during SCs. Thus, we would expect HAD to show the greatest fraction of extreme R to be related to SCs, compared to ESK and LER.

To explore this further, Figure 3 shows the percentage of the data set above different thresholds of R that occur during SCs. Figure 3 is plotted as a function of percentile of R to make the three stations directly comparable. The values of the marked percentiles for each station are provided at the top for context. At ESK 2–2.5% of the values of R that are greater than that the 99.8th percentile occur during SCs, and this percentage is fairly consistent moving toward larger percentiles. A similar result can be seen for LER where $\sim 0.75\%$ of the values of R that exceed the 99.8th percentile (and higher) are recorded during SCs. In contrast, at HAD the percentage of R values greater than a given percentile increases from 2.5% at the 99.8th percentile up to a maximum of $\sim 8\%$ for values of R above the 99.99th percentile. In context, using the values of the percentiles at the top, at HAD $\geq 5\%$ of the values of R that exceed ~ 20 nT/min can be explained by SCs.

Conversely, at the lowest latitude station, HAD, the vast majority ($\geq 90\%$) of the extreme values of R are caused by phenomena other than SCs. At higher latitudes, over 97.5% and 99% of the extreme values of R (i.e., ≥ 99.97 th percentile) are not related directly to SCs, at ESK and LER, respectively. However, SCs are known to often be followed by further magnetospheric activity, driven by the sharp increase in solar wind dynamic

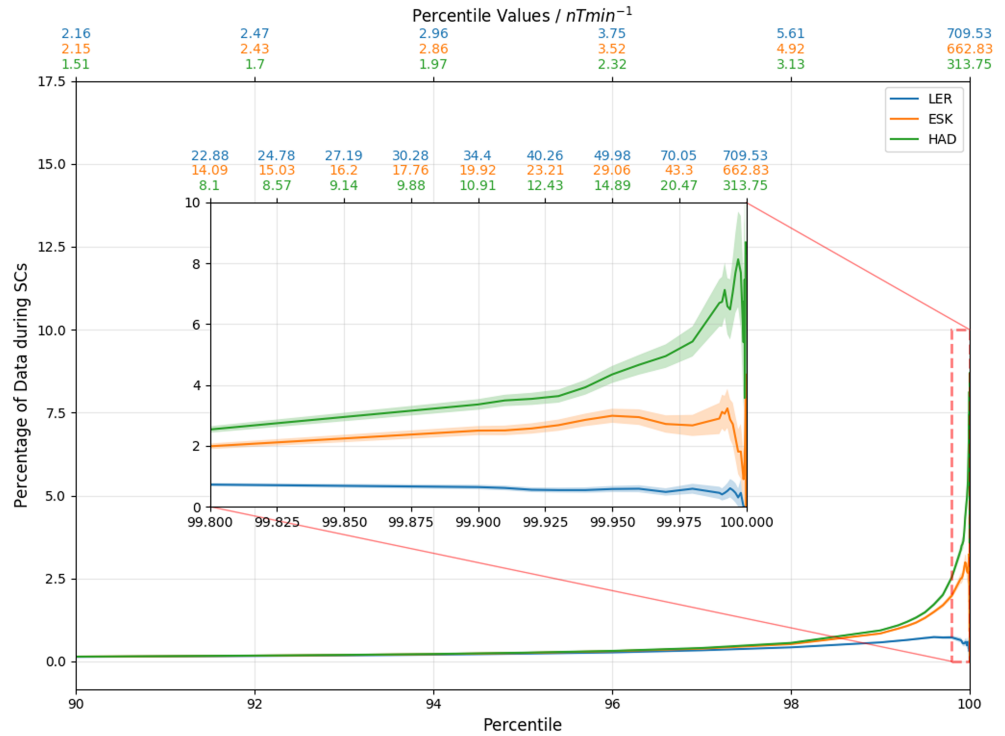


Figure 3. The percentage of data attributed to SCs that exceeds a percentile of the distribution of all R . The shaded region shows $\pm 68.27\%$ confidence interval, assuming the general Poisson distribution. The corresponding values of R for the marked percentiles are provided at the top for each station.

pressure. In particular the SSC subset of SCs is defined as those SCs which are followed by geomagnetic storms. Below we will evaluate SC-related activity following the event itself.

3.2. Statistics of R Related to SCs

Similar to Figure 2, Figure 4 shows PDFs of R from HAD, ESK, and LER, with the addition of distributions corresponding to data obtained within the 24 hr following an SC (orange), and the data unrelated to any activity following an SC (blue). The “unrelated” data set is composed of all intervals that begin 7 days following the onset of one SC extending to the onset of the next SC.

Inspecting the top row of Figure 4, for almost all values of R , the PDFs of the 24 hr following an SC (orange) are intermediate between the overall PDF (black) and the SC subset (red). Below $R \sim 2$ nT/min the probability density is greater than that found during SC intervals, while above this point the probability density is less than that observed during SCs. The difference between the SC intervals and the following day above $R \sim 2$ nT/min is greatest at HAD, while at LER the two distributions are most similar. Removing any data related to SCs or the days following, the unrelated PDF in blue, displays a smaller value of the PDF at values of $R \geq 10$ nT/min, compared to the complete data (in black).

The lower panels of Figure 4 show the ratio of the PDFs of subsets of the data to the overall distribution. The chosen subsets are the data unrelated to SCs, during SCs, and in the intervals 24 hr after an SC. For all three stations the data unrelated to SCs (blue) comprise the majority of the data set (i.e., are constant at a ratio of ~ 1) below $R \sim 2$ nT/min. Above $R \sim 2$ nT/min the unrelated distribution drops rapidly: The relative probability of large R at times unrelated to SCs is fairly low. This is most evident at HAD, while LER shows the smallest dropoff. Meanwhile, during SCs (in red) the probability density of large values of R is greatly enhanced. At HAD and ESK values of R greater than 10 nT/min are over 100 times more likely, while at LER they are around 30–40 times more likely. Also, in the 24 hr following an SC values exceeding 10 nT/min are over 10 times more likely at all stations.

The length of a geomagnetic storm is not fixed, and there is a delay between an SSC and the minimum value of $Dst/Sym-H$. To explore the effect of such delayed activity Figure 5 shows how the values of the 90th, 99th, and 99.97th percentiles vary with the number of days following an SC. On the time axis, a value

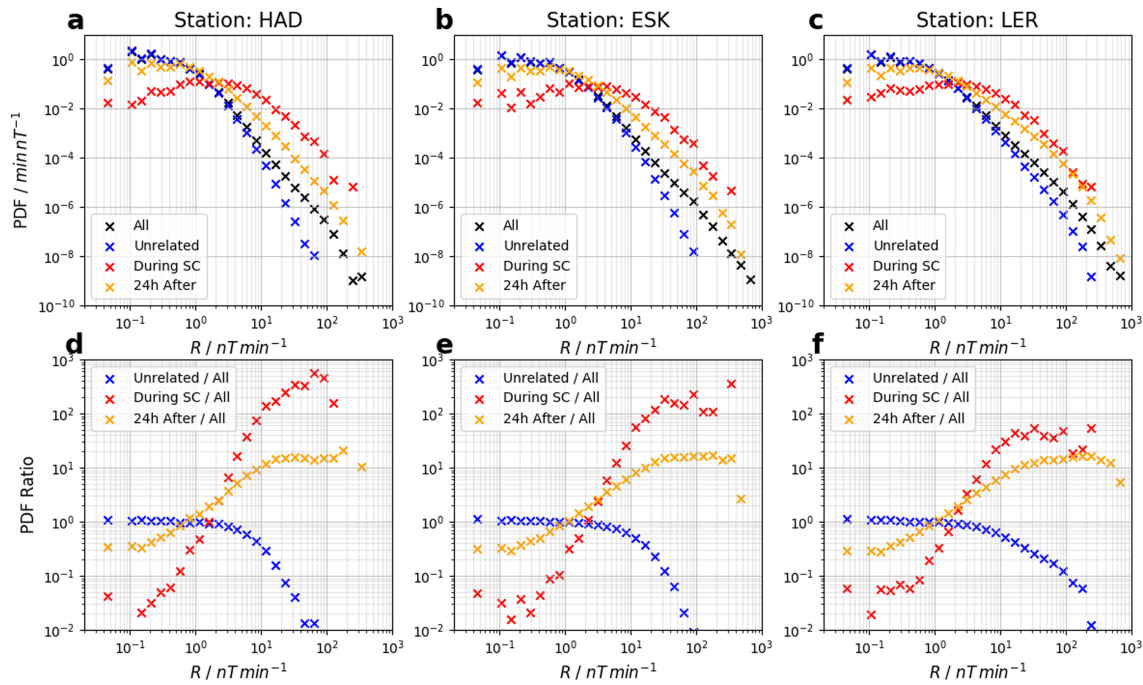


Figure 4. (a–c) PDFs of R for the full data set (black), during SCs (red), the interval 24 hr following an SC (orange), and data unrelated to SCs (blue). (d–f) The ratio of the PDFs at each value of R to the total data set. From left to right the columns represent the data collected at the HAD, ESK, and LER stations.

of 0 represents the few minutes defined as the SC itself, while a value of 1 then corresponds to the 24 hr following the SC, 2 to the period 24–48 hr following the end of the SC, and so on. The horizontal dashed lines in Figure 5 show the percentile values for the data unrelated to SCs (defined as above).

At HAD (Figure 5a) all three chosen percentiles are largest during the SC itself (“Day 0”), and then drop rapidly until they reach the background levels within 4 days of the SC. The same pattern is found for the ESK observations (Figure 5b). However, at LER (Figure 5c) the highest percentile (99.97th) is slightly greater during the 24 hr following the SC. With this exception, the percentiles at LER then drop until the fourth day following the SC, when the percentiles have returned to values comparable with the background.

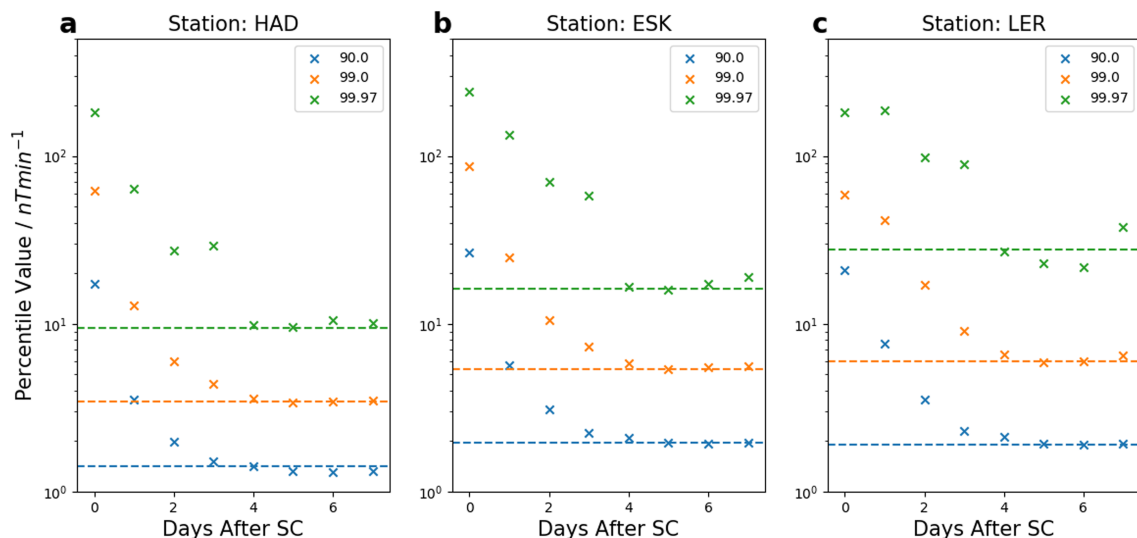


Figure 5. The variation in the 90th, 99th, and 99.97th percentiles of R as a function of time after a sudden commencement, presented for the HAD (a), ESK (b), and LER (c) stations. The horizontal dashed lines represent the percentiles obtained from intervals unrelated to SCs (defined as being at least 7 days after an SC).

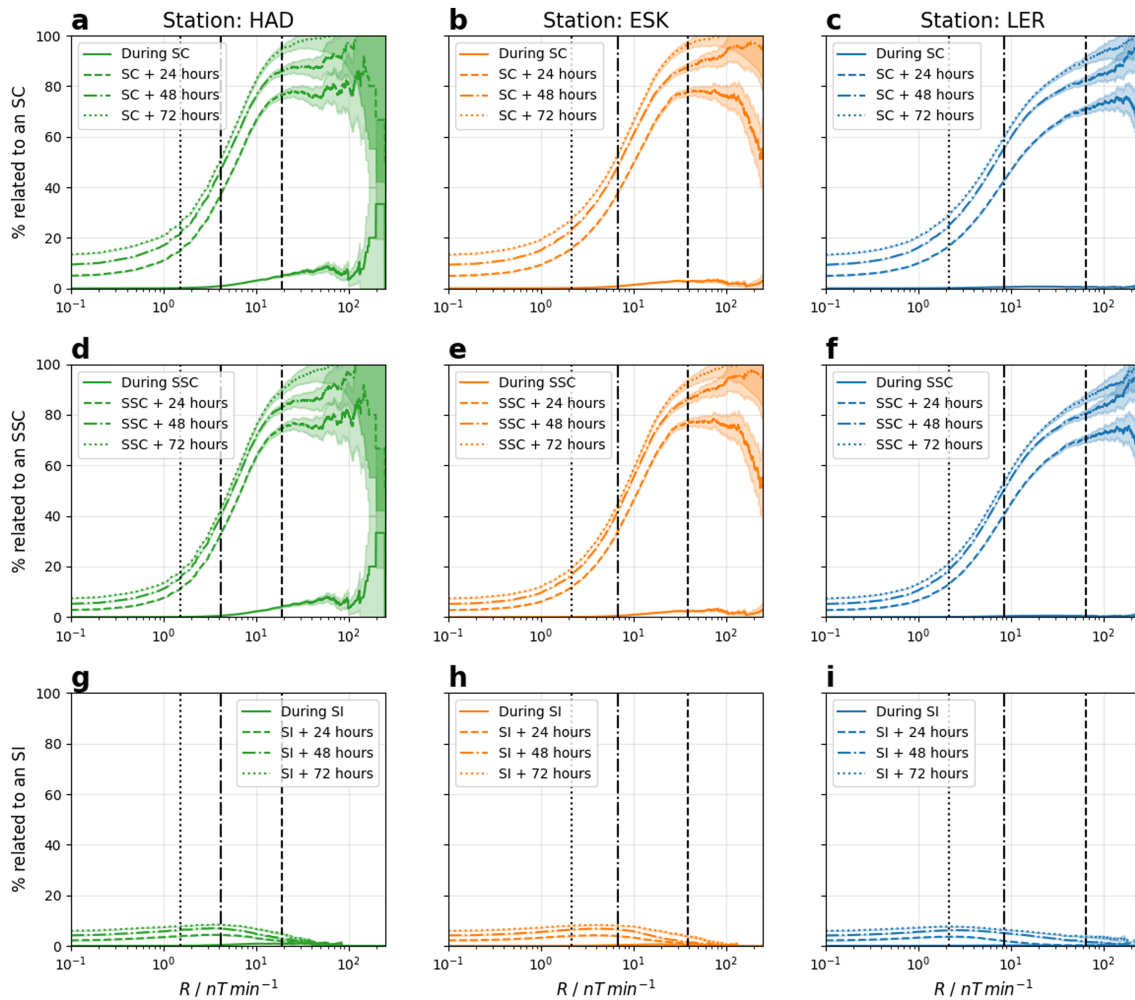


Figure 6. The percentage of all data that is recorded during or within 1–3 days of an SC (a–c), SSC (d–f), or SI (g–i), as a function of R for the HAD (a, d, g), ESK (b, e, h), and LER (c, f, i) stations. Format for each panel is similar to Figure 3. The vertical dotted, dot-dashed, and dashed lines represent the 90th, 99th, and 99.97th percentiles for all data from each station.

Figure 5 shows that the percentiles are elevated at all three stations for several days following the defined SC intervals. In addition to possessing elevated percentiles, these periods represent a much larger amount of data than the SCs themselves, and thus it is instructive to reassess the percentage of data related to SCs that exceeds percentiles/values of R (e.g., Figure 3) including the several days following SCs.

Similar to Figure 3, Figures 6a–6c show the percentage of all data exceeding a given value of R that is recorded either within an SC, or up to 3 days after an SC. The 3 day interval was selected from inspection of Figure 5: the enhanced R values related to SCs abates after a period of approximately 3 days. As a baseline, in the entire data set approximately 4%, 9%, and 13% of the data are within 1, 2, or 3 days of an SC respectively, that is, the values on the left of Figures 6a–6c. The vertical dotted, dashed, and dot-dashed lines show the 90th, 99th, and 99.97th percentiles of all data recorded at each station.

From Figures 6a–6c, SCs represent a very small portion of the data, and as discussed in the context of Figure 3, this holds at large R . In fact, the relatively sharp increase in percentage at HAD that appeared in Figure 3 (as a function of percentile) can be seen here to be relatively modest increase/plateau as a function of R . Taking this asymptotic behavior and extrapolating beyond the observed range would indicate that SCs themselves are likely of little importance for very extreme R (i.e., $R \geq$ several hundred nT) in the United Kingdom. The sharp increase in percentage above 100 nT/min at HAD corresponds to a level at which there is very little data (signified by the large shaded confidence interval).

Incrementally including the data from the days following the SC can be seen to increase the percentages dramatically at all three stations. The largest increase is found by including data from the 24 hr immediately following the SC. For each of these curves in turn, a much greater percentage of the data is associated with SCs as the value of R increases. For example, including the 24 hr following the SC (the dashed lines in Figures 6a–6c, above the 90th percentile between 15% and 17% of the data is associated with SCs. However, above the 99.97th percentile between 70% and 75% of the data above the 99.97th percentile are present. If the window following the SC is increased to 72 hr, the percentage of associated data above the 99.97th percentile rises to between 90% and 94%. Further, all $R \geq 200$ nT/min occurs within 3 days of an SC.

In general, the percentages in Figures 6a–6c can be seen to decrease slightly as the stations increase in latitude, that is, moving from (a) to (c). This is likely a result of the increased contribution of large R from auroral currents at the higher latitudes, for example, during substorms (Freeman et al., 2019).

3.3. Effect of SC Type on the Statistics of R

As discussed above, there are two classes of SC: SIs and SSCs, a split that is made ex post facto by examining the minimum Sym-H in the 24 hr following the SC. From the original 380 SCs, 215 are associated with a minimum Sym-H ≤ -50 nT in the following 24 hr and we therefore classify them as SSCs. It is reasonable to expect that SSCs would be associated with longer lasting, and possibly larger rates of change of the magnetic field, both during the SC itself and in the following interval.

Figures 6d–6f show the percentage of all data that are recorded during or up to 3 days after an SSC-type event, that exceeds a value of R . Figures 6g–6i show the same but for SI-type events. The format for each panel is similar to Figure 3. For SSC-type events it can be seen that they very closely resemble the top row of Figure 6 (plotted for all SCs): a very large fraction of the data exceeding the 99.97th percentile are recorded within 3 days of an SSC. In contrast, very little data at large R is associated with SI-type events (Figures 6g–6i). The percentages associated with SI-type events peak between the 90th and 99th percentiles at $\sim 8\%$ of the data (within 72 hr) at all three stations. An almost negligible amount of the data at large R ($\leq 1\%$ for the all plotted values) is associated with SI intervals. This comparison suggests that not only do SSCs cause greater initial values of R than SIs, but only they are followed by significantly high R in the next few days due to the geomagnetic storm.

4. Discussion

In this work the value of R (the rate of change of the horizontal component of the magnetic field) has been taken to be a proxy for the threat to U.K. power systems from GICs. However, the true magnitude of GICs is also dependent upon factors such as the relative geometry of the power grids and the local ground conductivity (Beggan, 2015; Thomson et al., 2005; Viljanen et al., 1999, 2013, 2014). Though large rates of change of the surface magnetic field are good predictors of GICs (Viljanen et al., 2001), significant power network impacts have been observed for relatively small rates of change (Kappenman, 2006). With this in mind we will now discuss the results concerning the rate of the change of the magnetic field, with respect to their latitude, and to their potential GIC impact on the U.K. power network.

4.1. Variation With Latitude of the SC-Related Rate of Change of the Surface Magnetic Field

Fiori et al. (2014) showed that, on a global scale, the rates of change associated with SCs increase with magnetic latitude up to a maximum at $\sim 65^\circ$, for the subset of events that show enhanced rates of change at high latitudes. This trend has been observed previously and suggested to be the result of a pair of traveling vortical currents, generated by the coupling of a compressional wave to a transverse Alfvén wave (Araki, 1994). Fiori et al. (2014) examined the change in the X component of the field, and suggest that it is the result of enhancement of the DP2 convection electrojets.

The HAD, ESK, and LER stations are found at magnetic latitudes of 47.37° , 52.74° , and 58.2° , respectively; these values were calculated using the International Geomagnetic Reference Field (IGRF) 2010 model. Therefore, the locations of these stations would suggest that they may show an increase in R from low to high latitudes. However, we have shown that during SC intervals the pattern of increasing R at larger latitudes is not present, and the percentiles of R instead maximize at ESK, the station at the middle latitude ($\sim 53^\circ$ magnetic latitude).

This result could be caused by either the latitudinal location of phenomena that drive large R or by differences in the ground conductivity local to the stations: The total measured magnetic perturbation is a combination of that produced by the external (e.g., ionospheric) and induced currents (in the solid Earth) (Tanskanen et al., 2001). Exploring the first option, the subauroral latitude of the ESK station would appear to argue against the convection electrojets being responsible for the largest values of R . Meanwhile, the compressional-Alfvén wave coupling model could be consistent with this result if the coupling occurred preferentially at subauroral latitudes; however, this would not explain the previous observations showing SC related field changes increasing toward the auroral zone (e.g., Araki, 1994; Fiori et al., 2014). Therefore, it is more likely that it is an effect of the ground conductivity local to the stations, either because the values of R at ESK are increased, or that the values of R at the highest latitude station (LER) are reduced/damped. A potentially important difference between the stations are their geographical locations: ESK is located on the U.K. mainland, while LER is located on the Shetland Islands, and so the magnetic perturbations from induced currents may be different due to differing conductivity of the geology and seawater (Beamish et al., 2002; Tanskanen et al., 2001). Interestingly, southern Scotland is known to be anomalously conductive around the ESK station (e.g., Hutton et al., 1977). The conductivity explanation is also supported by the fact that the ESK station has provided unexpectedly extreme results when considering the amplitude and return period of large field variability (Thomson et al., 2011), a result independent of any SC-related mechanism.

Another potential reason for the inconsistency of the result with previous studies is that we have employed the vector rate of change (R , defined in equation (1)), in contrast to the rate of change of the magnitude of \mathbf{H} used by Fiori et al. (2014). If the distinct definitions are causing the different results, then it would suggest that large field rotations are significant at the latitude of ESK during SCs. Future work should explore the prevalence of such large field rotations explicitly.

4.2. GIC Impact

SCs represent an important and potentially predictable cause of GICs in the United Kingdom and at similar geomagnetic latitudes. Currently, the shocks that result in SCs can be first observed by spacecraft at L1, providing less than 1 hr travel time to react and mitigate any potential GICs. In the future, it may be possible to predict some shocks from data collected at L5, providing a greatly increased window of opportunity. This work has shown that the probability of recording values of R greater than 10 nT/min are increased 30–100 times during SCs. However, they are very short lived and so contribute $\leq 8\%$ of potentially damaging R .

Instead, SCs are known to often be followed by prolonged magnetospheric activity that can result in damaging GICs (Clilverd et al., 2018; Pulkkinen et al., 2005). We have shown that, for the United Kingdom, the percentiles of R are elevated above background levels for 3 days following an SC. Therefore, if an SC can be predicted, then it can be said that the risk of significant GICs will last for approximately 3 days. During the first day following an SC values of R between 10 and several hundred nT/min are 10 times more likely to be measured. Further, if it can be forecast that the SC is likely to be followed by a geomagnetic storm, then the values of R will be greater and the risk of large R is extended to 3 days. Conversely, if it can be predicted that the shock will not cause a geomagnetic storm and will therefore result in an SI, then the likelihood of observing large R is lower.

Though these results have been derived with data from U.K.-based magnetometer stations, some of the results may be qualitatively extrapolated to systems at similar geomagnetic latitudes. However, this work has highlighted the importance of local effects in determining the precise magnitude of R , and so local studies are required to fully assess the vulnerabilities of a location. Nonetheless, a result that is likely to be more broadly applicable is the 3 day interval during which the largest R are observed following an SC. This result can be attributed to the nature of the phenomena that cause large R at this range of latitudes.

In this work we have considered the immediate impact of SCs, as well as the intervals that follow. However, we have not explored the effect of the local time of the station during such periods. The magnitude of dB/dt generated by interplanetary shocks has been shown to be dependent upon the local time of the station (e.g., Fiori et al., 2014; Oliveira et al., 2018), and therefore the local time of a region may further act to enhance or reduce the risk of a large GIC. Future work should explore the effect of the local time on the magnitude of R .

5. Summary

In this work we have analyzed the rate of change of the horizontal component of the magnetic field (R , defined as in equation (1)) at three magnetometer stations spanning the latitudinal extent of the United Kingdom during intervals related to SCs between 1996 and 2016. SCs are identifiable in ground based magnetometer data as sharp deflections in the horizontal components of the magnetic field, related to the impact of a solar wind pressure pulse on the magnetosphere. Large rates of change of the horizontal ground magnetic field are associated with potentially damaging ground induced currents (GICs) in power networks.

We have shown that the distributions of R during SCs are statistically shifted to larger values than the distributions for the full data set. Rates of change greater than 10 nT/min are 30–100 times more likely during SCs. The lowest latitude station (HAD) shows the greatest shift relative to the original distribution. The percentiles of R are largest at the ESK station, and not the highest latitude station (LER) as may have been expected. A maximum of 8% of the potentially damaging values of R are attributable to SCs at HAD, the lowest latitude station, and this percentage reduces significantly with increasing latitude. At the highest latitude station only a maximum of $\sim 0.75\%$ of the extreme R values occur during SCs.

The sudden pressure increase that causes SCs can also have other effects, such as triggering geomagnetic storms. We find that the percentiles of R recorded for 3 days following the SC are much greater than background levels. Indeed, in the 24 hr following an SC values of R between 10 and several hundred nT/min are 10 times more likely than during any random interval. Additionally, between 90% and 94% of the data above the 99.97th percentile occurs within 3 days of an SC, depending on the station. All values of $R \geq 200$ nT/min occur within 3 days of an SC. Further, subdividing the SCs by whether they are followed by a geomagnetic storm reveals that those that are followed by a storm show larger values of R during the SC itself, and are also the only type that are followed by the 3 day interval of enhanced R .

Acknowledgments

The magnetometer data used in this study were collected at the Hartland, Eskdalemuir, and Lerwick observatories. We thank the British Geological Survey for supporting their operation and INTERMAGNET for promoting high standards of magnetic observatory practice. The data were downloaded from www.intermagnet.org and are freely available there. We acknowledge and thank NASA GSFC's Space Physics Data Facility's OMNIWeb (or CDAWeb or ftp) service for the use of OMNI data (<https://omniweb.gsfc.nasa.gov>). The results presented in the paper also rely on the SC list made available by the International Service on Rapid Magnetic Variations (<http://www.obsebre.es/en/rapid>) and published by the Observatorio de l'Ebre in association with the International Association of Geomagnetism and Aeronomy (IAGA) and the International Service of Geomagnetic Indices (ISGI). We thank the involved national institutes, the INTERMAGNET network and the ISGI. A. W. S. and I. J. R. were supported by STFC Consolidated Grant ST/S000240/1 and NERC Grant NE/P017150/1. C. F. was supported by the NERC Independent Research Fellowship NE/N014480/1 and STFC Consolidated Grant ST/S000240/1. M. P. F. was supported by NERC Grant NE/P016693/1. The analysis in this paper was performed using python, including the pandas, numpy, scipy, and matplotlib libraries.

References

- Akasofu, S. I. (1964). The development of the auroral substorm. *Planetary and Space Science*, 12(4), 273–282. [https://doi.org/10.1016/0032-0633\(64\)90151-5](https://doi.org/10.1016/0032-0633(64)90151-5)
- Araki, T. (1977). Global structure of geomagnetic sudden commencements. *Planetary and Space Science*, 25(4), 373–384. [https://doi.org/10.1016/0032-0633\(77\)90053-8](https://doi.org/10.1016/0032-0633(77)90053-8)
- Araki, T. (1994). A Physical Model of the Geomagnetic Sudden Commencement. In M. Engebretson, K. Takahashi, & M. Scholer (Eds.), *Solar wind sources of magnetospheric ultra-low-frequency waves* (Chap. 16, p. 183).
- Araki, T., Keika, K., Kamei, T., Yang, H., & Alex, S. (2006). Nighttime enhancement of the amplitude of geomagnetic sudden commencements and its dependence on IMF-Bz. *Earth, Planets and Space*, 58(1), 45–50. <https://doi.org/10.1186/BF03351912>
- Beamish, D., Clark, T., Clarke, E., & Thomson, A. (2002). Geomagnetically induced currents in the UK: geomagnetic variations and surface electric fields. *Journal of Atmospheric and Solar-Terrestrial Physics*, 64(16), 1779–1792. <https://www.sciencedirect.com/science/article/pii/S136468260200127X>, [https://doi.org/10.1016/S1364-6826\(02\)00127-X](https://doi.org/10.1016/S1364-6826(02)00127-X)
- Beggan, C. D. (2015). Sensitivity of geomagnetically induced currents to varying auroral electrojet and conductivity models. *Earth, Planets and Space*, 67, 24. <http://www.earth-planets-space.com/content/67/1/24>, <https://doi.org/10.1186/s40623-014-0168-9>
- Beland, J., & Small, K. (2004). Space weather effects on power transmission systems: The cases of Hydro-Quebec and transpower NewZealand Ltd [Proceedings Paper]. In I. Daglis (Ed.), *Effects of space weather on technology infrastructure*, PO BOX 17, 3300 AA DORDRECHT (Vol. 176, pp. 287–299). Netherlands: Springer.
- Bolduc, L. (2002). GIC observations and studies in the Hydro-Québec power system. *Journal of Atmospheric and Solar-Terrestrial Physics*, 64(16), 1793–1802. <http://linkinghub.elsevier.com/retrieve/pii/S1364682602001281>, [https://doi.org/10.1016/S1364-6826\(02\)00128-1](https://doi.org/10.1016/S1364-6826(02)00128-1)
- Bolduc, L., Langlois, P., Boteler, D., & Pirjola, R. (1998). A study of geoelectromagnetic disturbances in Quebec. I. General results. *IEEE Transactions on Power Delivery*, 13(4), 1251–1256. <http://ieeexplore.ieee.org/document/714492/doi>, <https://doi.org/10.1109/61.714492>
- Boteler, D. (2014). Methodology for simulation of geomagnetically induced currents in power systems. *Journal of Space Weather and Space Climate*, 4, A21. <https://doi.org/10.1051/swsc/2014018>
- Boteler, D. H. (2003). Geomagnetic hazards to conducting networks. *Natural Hazards*, 28(2-3), 537–561. <https://doi.org/10.1023/A:1022902713136>
- Boteler, D. H., Pirjola, R. J., & Nevanlinna, H. (1998). The effects of geomagnetic disturbances on electrical systems at the Earth's surface. *Advances in Space Research*, 22(1), 17–27. <http://linkinghub.elsevier.com/retrieve/pii/S027311779701096X>, [https://doi.org/10.1016/S0273-1177\(97\)01096-X](https://doi.org/10.1016/S0273-1177(97)01096-X)
- Bothmer, V., Kallenbach, R., Klecker, B., & Marsch, E. (1999). The Solar Origin of Corotating Interaction Regions and Their Formation in the Inner Heliosphere. *Space Science Reviews*, 89, 141–178. <https://deepblue.lib.umich.edu/handle/2027.42/43796>, <https://doi.org/10.1023/A>
- Carter, B. A., Pradipta, R., Zhang, K., Yizengaw, E., Halford, A. J., & Norman, R. (2015). Interplanetary shocks and the resulting geomagnetically induced currents at the equator. *Geophysical Research Letters*, 42, 6554–6559. <https://agupubs.onlinelibrary.wiley.com/doi/pdf/10.1002/2015GL065060>, <https://doi.org/10.1002/2015gl065060>
- Chapman, S., & Ferraro, V. C. A. (1931). A New Theory of Magnetic Storms. *Terrestrial Magnetism and Atmospheric Electricity*, 36(2), 77. <https://doi.org/10.1029/TE036i002p00077>
- Chapman, S., & Ferraro, V. C. A. (1932). A new theory of magnetic storms. *Journal of Geophysical Research*, 37(2), 147. <https://doi.org/10.1029/TE037i002p00147>

- Chree, C. (1925). The times of "Sudden Commencements" (S.C.s) of magnetic storms: Observation and theory. *Proceedings of the Physical Society of London*, 38(1), 35–46. <http://stacks.iop.org/1478-7814/38/i=1/a=305?key=crossref.ddd5862873bdd55549f24a7b09002eda>, <https://doi.org/10.1088/1478-7814/38/1/305>
- Ciliverd, M. A., Rodger, C. J., Brundell, J. B., Dalzell, M., Martin, I., Mac Manus, D. H., & Obana, Y. (2018). Long-Lasting Geomagnetically Induced Currents and Harmonic Distortion Observed in New Zealand During the 7–8 September 2017 Disturbed Period. *Space Weather*, 16(6), 704–717. <https://doi.org/10.1029/2018SW001822>
- Curto, J. J., Araki, T., & Alberca, L. F. (2007). Evolution of the concept of Sudden Storm Commencements and their operative identification. *Earth, Planets and Space*, 59(11), i–xii. <https://doi.org/10.1186/BF03352059>
- Fiori, R. A. D., Boteler, D. H., & Gillies, D. M. (2014). Assessment of GIC risk due to geomagnetic sudden commencements and identification of the current systems responsible. *Space Weather*, 12, 76–91. <https://doi.org/10.1002/2013SW000967>
- Freeman, M. P., Forsyth, C., & Rae, I. J. (2019). The influence of substorms on extreme rates of change of the surface horizontal magnetic field in the U.K. *Space Weather*, 2018SW002148. <https://doi.org/10.1029/2018SW002148>
- Gonzalez, W. D., Joselyn, J. A., Kamide, Y., Kroehl, H. W., Ros, G., Tsuru, B. T., & Vasyliunas, V. M. (1994). *What is a geomagnetic storm?* (Vol.99; Tech. Ref. No. A4). doi: <https://doi.org/10.1029/93JA02867>
- Gosling, J., & Pizzo, V. (1999). Formation and Evolution of Corotating Interaction Regions and their Three Dimensional Structure. *Space Science Reviews*, 89(1/2), 21–52. <https://doi.org/10.1023/A:1005291711900>
- Harrison, R. A., Davies, J. A., Biesecker, D., & Gibbs, M. (2017). The application of heliospheric imaging to space weather operations: Lessons learned from published studies. *Space Weather*, 15, 985–1003. <https://doi.org/10.1002/2017SW001633>
- Hutton, V. R. S., Sik, J. M., & Gough, D. I. (1977). Electrical conductivity and tectonics of Scotland. *Nature*, 266(5603), 617–620. <https://doi.org/10.1038/266617a0>
- Kappenman, J. G. (1996). Geomagnetic storms and their impact on power systems. *IEEE Power Engineering Review*, 16(5), 5. <https://doi.org/10.1109/MPER.1996.491910>
- Kappenman, J. G. (2003). Storm sudden commencement events and the associated geomagnetically induced current risks to ground-based systems at low-latitude and midlatitude locations. *Space Weather*, 1(3), 1016. <https://doi.org/10.1029/2003SW000009>
- Kappenman, J. G. (2005). An overview of the impulsive geomagnetic field disturbances and power grid impacts associated with the violent Sun–Earth connection events of 29–31 October 2003 and a comparative evaluation with other contemporary storms. *Space Weather*, 3, S08C01. <https://doi.org/10.1029/2004SW000128>
- Kappenman, J. G. (2006). Great geomagnetic storms and extreme impulsive geomagnetic field disturbance events – An analysis of observational evidence including the great storm of May 1921. *Advances in Space Research*, 38(2), 188–199. <https://www.sciencedirect.com/science/article/pii/S0273117705012111?via%3Dihub>, <https://doi.org/10.1016/J.ASR.2005.08.055>
- Kappenman, J. G., & Albertson, D. (1990). Bracing for the geomagnetic storms. *IEEE Spectrum*, 27(3), 27–33. <https://doi.org/10.1109/6.48847>
- Kikuchi, T., Tsunomura, S., Hashimoto, K., & Nozaki, K. (2001). Field-aligned current effects on midlatitude geomagnetic sudden commencements. *Journal of Geophysical Research*, 106(A8), 15,555–15,565. <https://doi.org/10.1029/2001JA900030>
- Lehtinen, M., & Pirjola, R. (1985). Currents produced in earth conductor networks by geomagnetically-induced electric fields. *Annales Geophysicae*, 3(4), 479–484. <https://ci.nii.ac.jp/naid/10024499668/>
- Lühr, H., Schlegel, K., Araki, T., Rother, M., & Förster, M. (2009). Night-time sudden commencements observed by CHAMP and ground-based magnetometers and their relationship to solar wind parameters. *Annales Geophysicae*, 27(5), 1897–1907. <https://doi.org/10.5194/angeo-27-1897-2009>
- Marshall, R. A., Dalzell, M., Waters, C. L., Goldthorpe, P., & Smith, E. A. (2012). Geomagnetically induced currents in the New Zealand power network. *Space Weather*, 10, S08003. <https://doi.org/10.1029/2012SW000806>
- Mayaud, P. N. (1973). A hundred year series of geomagnetic data, 1868–1967: indices aa, storm sudden commencements (SSC). *IUGG Publ. Office*, 256.
- McPherron, R. L., Aubry, M. P., Russell, C. T., & Coleman, P. J. (1973). *Satellite Studies of Magnetospheric Substorms on August 15, 1968 4. Ogo 5 Magnetic Field Observations* (Vol.78; Tech. Ref. No. 26). <https://www.researchgate.net/profile/RobertMcPherron/publication/254933902?urlscore=&urlscore=Satellite&urlscore=Studies&urlscore=of&urlscore=Magnetospheric&urlscore=Substorms&urlscore=on&urlscore=August&urlscore=15&urlscore=1968/links/5adf4d5aa6fdcc29358e13ed/Satellite-Studies-of-Magnetospheric-Substorms-on-August-15-1968.pdf>
- Ngwira, C. M., Pulkkinen, A., Leila Mays, M., Kuznetsova, M. M., Galvin, A. B., Simunac, K., & Gloer, A. (2013). Simulation of the 23 July 2012 extreme space weather event: What if this extremely rare CME was Earth directed? *Space Weather*, 11, 671–679. <https://doi.org/10.1002/2013SW000990>
- Oliveira, D. M., Arel, D., Raeder, J., Zesta, E., Ngwira, C. M., Carter, B. A., & Gjerloev, J. W. (2018). Geomagnetically Induced Currents Caused by Interplanetary Shocks With Different Impact Angles and Speeds. *Space Weather*, 16, 636–647. <https://doi.org/10.1029/2018SW001880>
- Pulkkinen, A., Bernabeu, E., Eichner, J., Beggan, C., & Thomson, A. W. P. (2012). Generation of 100-year geomagnetically induced current scenarios. *Space Weather*, 10, S04003. <https://doi.org/10.1029/2011sw000750>
- Pulkkinen, A., Lindahl, S., Viljanen, A., & Pirjola, R. (2005). Geomagnetic storm of 29–31 October 2003: Geomagnetically induced currents and their relation to problems in the Swedish high-voltage power transmission system. *Space Weather*, 3, S08C03. <https://doi.org/10.1029/2004SW000123>
- Reeves, G. D., McAdams, K. L., Friedel, R. H. W., & O'Brien, T. P. (2003). Acceleration and loss of relativistic electrons during geomagnetic storms. *Geophysical Research Letters*, 30(10), 1529. <https://doi.org/10.1029/2002GL016153>
- Takeuchi, T., Araki, T., Viljanen, A., & Watermann, J. (2002). Geomagnetic negative sudden impulses: Interplanetary causes and polarization distribution. *Journal of Geophysical Research*, 107(A7), 1096. <https://doi.org/10.1029/2001JA900152>
- Tanskanen, E. I., Viljanen, A., Pulkkinen, T. I., Pirjola, R., Häkkinen, L., Pulkkinen, A., & Amm, O. (2001). At substorm onset, 40% of AL comes from underground. *Journal of Geophysical Research*, 106(A7), 13,119–13,134. <https://doi.org/10.1029/2000JA900135>
- Thomson, A. W., Dawson, E. B., & Reay, S. J. (2011). Quantifying extreme behavior in geomagnetic activity. *Space Weather*, 9, S10001. <https://doi.org/10.1029/2011SW000696>
- Thomson, A. W., McKay, A. J., Clarke, E., & Reay, S. J. (2005, nov). Surface electric fields and geomagnetically induced currents in the Scottish Power grid during the 30 October 2003 geomagnetic storm. *Space Weather*, 3, S11002. <https://doi.org/10.1029/2005sw000156>
- Turner, D. L., O'Brien, T. P., Fennell, J. F., Claudepierre, S. G., Blake, J. B., Kilpua, E. K. J., & Hietala, H. (2015). The effects of geomagnetic storms on electrons in Earth's radiation belts. *Geophysical Research Letters*, 42, 9176–9184. <https://doi.org/10.1002/2015GL064747>
- Viljanen, A., Amm, O., & Pirjola, R. (1999). Modeling geomagnetically induced currents during different ionospheric situations. *Journal of Geophysical Research*, 104(A12), 28,059–28,071. <https://doi.org/10.1029/1999JA900337>

- Viljanen, A., Nevanlinna, H., Pajunpää, K., & Pulkkinen, A. (2001). Time derivative of the horizontal geomagnetic field as an activity indicator. *Annales Geophysicae*, *19*(9), 1107–1118. <https://doi.org/10.5194/angeo-19-1107-2001>
- Viljanen, A., Pirjola, R., Prácer, E., Ahmadzai, S., & Singh, V. (2013). Geomagnetically induced currents in Europe: Characteristics based on a local power grid model. *Space Weather*, *11*, 575–584. <https://doi.org/10.1002/swe.20098>
- Viljanen, A., Pirjola, R., Prácer, E., Katkalov, J., & Wik, M. (2014). Geomagnetically induced currents in Europe. *Journal of Space Weather and Space Climate*, *4*, A09. <https://doi.org/10.1051/swsc/2014006>
- Zhang, J. J., Wang, C., Sun, T. R., Liu, C. M., & Wang, K. R. (2015). GIC due to storm sudden commencement in low-latitude high-voltage power network in China: Observation and simulation. *Space Weather*, *13*, 643–655. <https://doi.org/10.1002/2015SW001263>
- Zhao, X., & Dryer, M. (2014). Current status of CME/shock arrival time prediction. *Space Weather*, *12*, 448–469. <https://doi.org/10.1002/2014SW001060>